Compact MIMO Antenna for Portable Devices in UWB Applications

Li Liu, S. W. Cheung, *Senior Member, IEEE*, and T. I. Yuk

***Abstract*—A compact multiple-input-multiple-output (MIMO) antenna with a small size of 26×40 mm^2 is proposed for portable ultrawideband (UWB) applications. The antenna consists of two planar-monopole (PM) antenna elements with microstrip-fed printed on one side of the substrate and placed perpendicularly to each other to achieve good isolation. To enhance isolation and increase impedance bandwidth, two long protruding ground stubs are added to the ground plane on the other side and a short ground strip is used to connect the ground planes of the two PMs together to form a common ground. Simulation and measurement are used to study the antenna performance in terms of reflection coefficients at the two input ports, coupling between the two input ports, radiation pattern, realized peak gain, efficiency and envelope correlation coefficient for pattern diversity. Results show that the MIMO antenna has an impedance bandwidth of larger than 3.1–10.6 GHz, low mutual coupling of less than -15 dB, and a low envelope correlation coefficient of less than 0.2 across the frequency band, making it a good candidate for portable UWB applications.**

***Index Terms*—Multiple-input-multiple-output (MIMO) antenna, pattern diversity, planar monopole, ultrawideband (UWB).**

I. Introduction

ULTRAWIDEBAND (UWB) is a rapidly growing technology which makes use of wide frequency band to transmit signals at low energy level. It has promising applications in short-range high-data-rate transmission, radar imaging and cancer sensing, etc. Since the authorization from the Federal Communications Commission (FCC) in the US for the unlicensed use of 3.1–10.6 GHz spectrum for applications with low power emission in 2002 [1], UWB systems have attracted much attention. Like other wireless communication systems, UWB systems suffer from multipath fading. It is well-known that multiple-input-multiple-output (MIMO) technology can be used to provide multiplexing gain and diversity gain to improve the capacity and link quality, respectively, of wireless systems [2]. UWB systems using huge bandwidths already have high data rates, so MIMO technology can be used for fade countermeasure through diversity gain. The basic concept of MIMO/diversity is to use multiple antenna elements to transmit or receive signals with different fading characteristics. Since it is unlikely that all the received signals will experience deep fading at the same time, the system reliability can be increased by proper selection/combining of the received signals. However, installing multiple antenna elements on the small space available in portable devices will inevitably cause severe mutual coupling and significantly degrade the diversity performance. Thus, one of the main challenges to employ MIMO technology in portable devices is the design of the small MIMO antennas with low mutual coupling.

Many MIMO antennas have been proposed for UWB systems [3]–[16]. In [3]–[10], various decoupling structures were employed between two symmetrically placed elements to enhance isolation. In [11], [12], antenna elements of different types were combined to achieve pattern diversity. The antenna elements had distinct radiation patterns and polarizations, and so were able to receive signals with low correlation. In [13]–[16], perpendicular feeding directions were used to achieve polarization and pattern diversity. Among the aforementioned designs, some were not able to operate in the entire UWB band allocated by the FCC [3], [4], [7], [11], [12]. For those which could cover the entire UWB band [5], [6], [8]–[10], [13]–[16], some were not compact enough for portable devices [13]–[15]. For example, in [13], a complicated 3-D feeding network with a large volume was required. In [14], [15], the sizes of the MIMO antennas were 80×80 mm^2. For the rest of these designs, the MIMO antenna proposed in [6] had the smallest size of $35 \times 40 = 1400$ mm^2. Good isolation was achieved by inserting a tree-like structure between the two antenna elements.

In this paper, an UWB MIMO antenna with a bandwidth from 3.1 to 10.6 GHz is proposed. It has a compact size of $26 \times 40 = 1040$ mm^2, about 25% smaller than the one in [6]. Two planar-monopole (PM) antenna elements with microstrip-fed are placed perpendicularly to each other. Two long ground stubs serving as parasitic monopoles and a short ground strip are used to enhance isolation and bandwidth. The simulated and measured performances show that the MIMO antenna is a good candidate for portable UWB applications.

II. Antenna Design

The geometry of the proposed UWB MIMO antenna, with an overall size of only $W \times L = 40 \times 26$ mm^2, is shown in Fig. 1. It is designed on a Rogers substrate, RO4350B, with a thickness of 0.8 mm, a permittivity of 3.5, and a loss tangent of 0.004. The antenna consists of two planar-monopole (PM) antenna elements, denoted as PM 1 and PM 2 in Fig. 1, with microstrip-fed through ports 1 and 2, respectively. The two PMs

Manuscript received January 13, 2013; revised March 25, 2013; accepted May 07, 2013. Date of publication May 15, 2013; date of current version July 31, 2013.

The authors are with the Department of Electrical and Electronic Engineering, The University of Hong Kong, Hong Kong, China (e-mail: liuli@eee.hku.hk; swcheung@eee.hku.hk; tiyuk@eee.hku.hk).

Color versions of one or more of the figures in this paper are available online at http://ieeexplore.ieee.org.

Digital Object Identifier 10.1109/TAP.2013.2263277

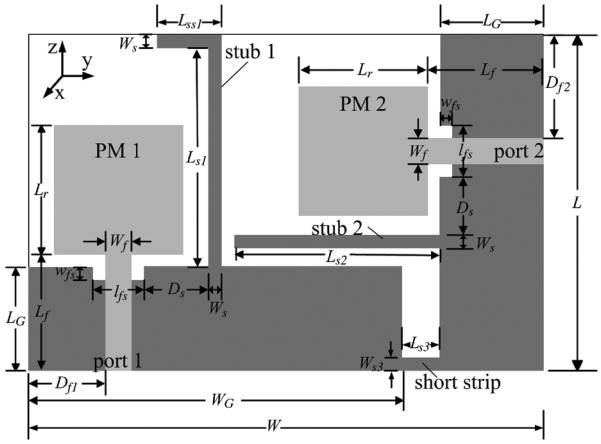

Fig. 1. Geometry of proposed antenna (top layer and bottom layer).

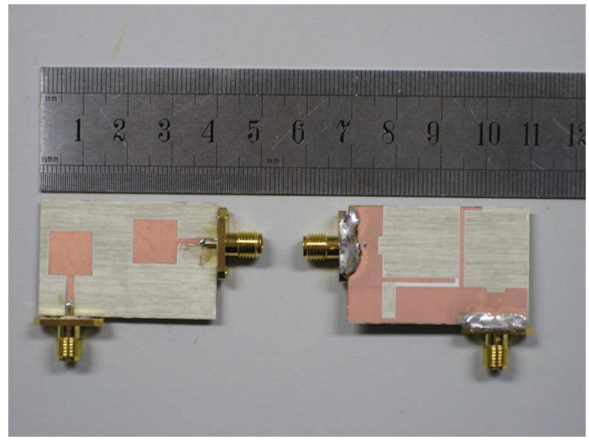

Fig. 2. Photograph of prototyped antenna.

TABLE I
DIMENSIONS OF PROPOSED ANTENNA (MM)

L	L_r	L_f	L_{s1}	L_{s2}	L_{s3}	l_{fs}	D_{f1}	D_s
26	10	9	17	16	3	4	6.1	5
W	L_G	W_f	W_s	L_{ss1}	W_{s3}	w_{fs}	D_{f2}	W_G
40	8	1.8	1	5	1	1	8.1	29

are printed perpendicularly to each other to provide good isolation between the two input ports. The two square-shaped radiators have identical dimensions with the side length of L_r and are printed on one side of the substrate. Each of the radiators is fed by a 50-Ω microstrip line with a dimension of $W_f \times L_f$. The ground planes of PM 1 and PM 2 have the same width of L_G but different lengths of W_G and L, respectively, and are printed on the other side of the substrate. A short ground strip with a size of $L_{s3} \times W_{s3}$ is used to electrically connect the two ground planes together, forming an L-shaped common ground for both PMs. For better impedance matching at high frequencies, a small rectangular slot with a size of $l_{fs} \times w_{fs}$ is cut on the upper edge of the ground plane underneath each feed line. To further enhance isolation and increase impedance bandwidth, two long ground stubs, stubs 1 and 2 as shown in Fig. 1, are employed. Stub 1 is placed in parallel with PM 1 and is bent to reduce the overall antenna area, while stub 2 is a simple straight stub placed in parallel with PM 2. Computer simulation using the EM simulation tool CST is carried out to study and optimize the proposed MIMO antenna, in terms of impedance bandwidths, radiation patterns and peak gains with input signal at either of the two input ports, and isolation between the two input ports. In simulation, the waveguide ports are used and the mesh lines per wavelength are set to be 30. Results have shown that a higher mesh setting would produce almost the same results. The optimized dimensions for the MIMO antenna are listed in Table I and used to fabricate the prototype as shown in Fig. 2 for measurement.

III. EFFECTS OF GROUND STUBS AND STRIP

In the MIMO antenna shown in Fig. 1, the short ground strip used to connect the two ground planes together and the two long ground stubs placed next to the radiators of PM 1 and PM 2 are critical for achieving the desirable performance in terms of isolation and impedance matching. Thus, computer simulation using the EM simulation tool CST has been used to study their effects on the antenna performance.

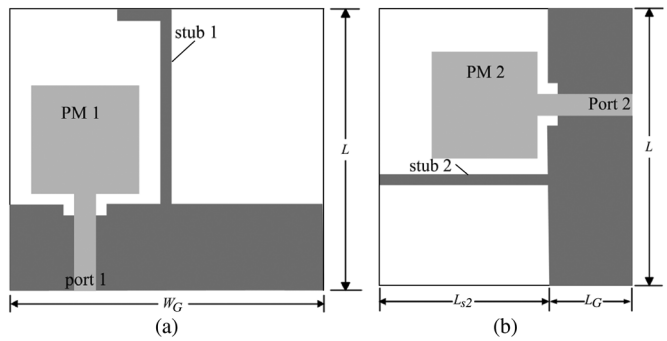

Fig. 3. Geometries of UWB monopole elements used in MIMO antenna. (a) PM 1 and (b) PM 2.

A. Effects of Long Ground Stubs

1) On Single Antenna Elements: The proposed MIMO antenna is composed of two UWB monopole elements, PM1 and PM 2, with the corresponding ground planes and long ground stubs serving as parasitic monopoles, as shown in Fig. 3. To gain more insight into the effects of the ground stubs on the impedance bandwidths, computer simulations are carried out on the two antenna elements with and without having the corresponding stubs. The simulated S_{11} of PM 1, PM 1 with stub 1, PM 2, and PM 2 with stub 2 are shown in Fig. 4. It can be seen that PM 1 without stub 1 has the lower cutoff frequency (for $S_{11} < -10$ dB) of 3.3 GHz and so cannot satisfy the requirement for UWB operation. Adding stub 1 to PM 1 can generate a resonance at 3.5 GHz and shift the lower cutoff frequency to 2.8 GHz. The antenna then can satisfy the UWB requirement. Similarly, PM 2 without stub 2 has a lower cutoff frequency (for $S_{22} < -10$ dB) of 4 GHz and so again cannot satisfy the requirement for UWB operation. When stub 2 is added, a resonance at 4.2 GHz is generated, which extends the lower cutoff frequency to 3.3 GHz. Although the bandwidth still cannot cover the entire UWB, when the two antenna elements are connected together by using the short ground strip as shown in Fig. 1, additional resonances are generated which

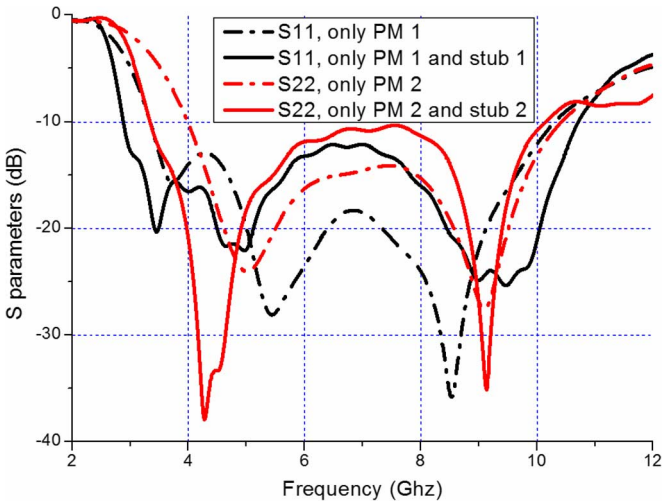

Fig. 4. Simulated S parameters for single antenna elements with and without long ground stubs.

extend the bandwidth towards the high and low frequencies, as will be shown later in Fig. 5(b).

2) On MIMO Antenna: The simulated S_{11}, S_{22} and S_{21} of the MIMO antenna are shown in Fig. 5(a), (b) and (c). To study the effects of the long ground stubs on the S-parameters of the antenna, the simulated S_{11}, S_{22} and S_{21} using only stub 1, only stub 2 or no stub are also shown in the same figure. Fig. 5(a) shows that using stub 2 alone has little effect on the impedance bandwidth for $S_{11} < -10$ dB, compared with the case without using any ground stub. However, when stub 1 is used (alone or together with stub 2), two strong resonances are generated at about 4.5 and 9 GHz. The strong resonance at 4.5 GHz moves the lower cutoff frequency from 4.4 GHz to about 2.9 GHz. This alters the frequency band from 4.4–10.1 GHz to 2.9–10.6 GHz and substantially increases the impedance bandwidth from 5.7 GHz to 7.7 GHz, respectively. (The frequency band from 3–3.5 GHz for using stub 1 alone has S_{11} only very slightly over 10 dB and so can be treated as passband.) For S_{22}, without using any of the ground stubs, Fig. 5(b) shows that the antenna has three relatively obvious resonances at 5.8, 7, and 8.9 GHz, which result in a wide impedance bandwidth of 3.5–10.1 GHz. However if only stub 1 is used, the resonance at 8.9 GHz disappears. As a result, the impedance bandwidth is reduced from 3.5–10.1 GHz to 3.4–8.5 GHz when compared with the case without using any stubs. When stub 2 alone is used, a resonance at 4 GHz is created, which increases the impedance bandwidth. When both ground stubs are used, four resonances are generated, with the lowest and highest ones at 2.9 and 10.1 GHz, respectively, resulting in a wide bandwidth of 2.8–10.8 GHz. Usually mutual coupling S_{21} of less than -15 dB is considered adequate for a good performance [6], [10], [14], [15]. Fig. 5(c) shows that, without using the stubs, the decoupling bandwidth for $S_{21} < -15$ dB is from 4.5–12 GHz. Stub 1 alone increases the decoupling bandwidth by suppressing S_{21} in the frequency band from 3–5 GHz and stub 2 alone has little effect on the decoupling bandwidth. Using stubs 1 and 2 together has the decoupling bandwidth better than using only stub 2 but worse than using only stub 1. However, in optimization, all three parameters, S_{11}, S_{22} and S_{21}, should be made to satisfy the requirement for UWB operation.

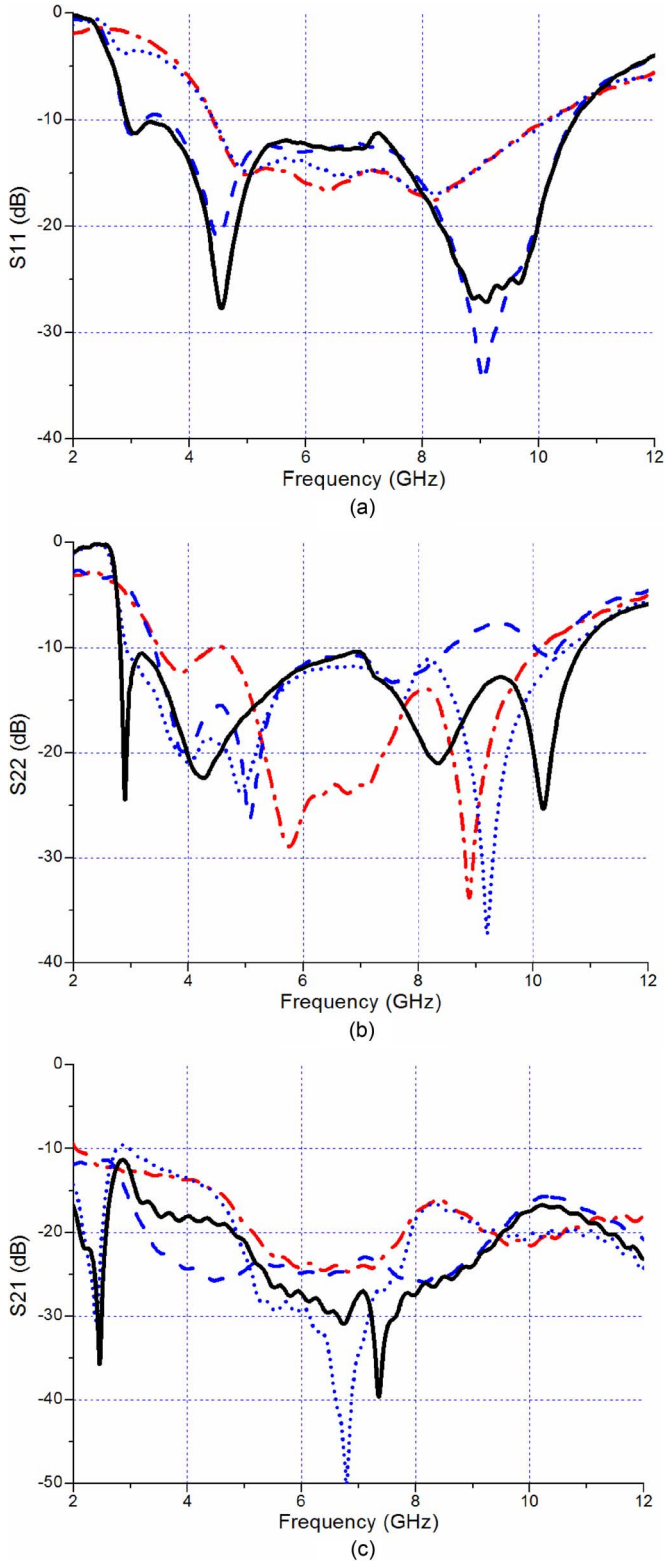

Fig. 5. Simulated (a) S_{11}, (b) S_{22}, and (c) S_{21}. (– · – with no ground stub, – – with only stub 1, · · · · · with only stub 2, ——— with both stubs).

It should be noted that stub 2 together with the ground plane forms an L-shaped slot (similar to the crescent slot used in [12])

which generates a resonance at a lower frequency of 2.5 GHz for S_{21} as shown in Fig. 5(c). This resonance in S_{21}, if shifted into the UWB, could be used to further reduce the mutual coupling between the two ports [12]. Thus, simulation studies have been carried out in attempts to use the dimensions of this L-shaped slot to move the resonance from 2.5 GHz into the UWB. The studies included shortening L_{s2} (the length of stub 2) and increasing W_{s3} (the width of the short ground strip). Unfortunately, results showed that both changes would increase the lower cutoff frequency for S_{22} and so the antenna could no longer satisfy the requirement for UWB operation.

Current distribution has been used to further study the operation of the MIMO antenna. Fig. 6 shows the simulated current distributions of the antenna with and without using the two stubs at 4.5 GHz and 8.5 GHz which are about the resonant frequencies for both S_{11} and S_{22}. Without using the two ground stubs, when port 1 is excited and port 2 is terminated with a 50-Ω load, Fig. 6(a) and (e) show that currents are coupled to the radiator of PM 2 and flow to port 2. When port 2 is excited and port 1 is terminated with a 50-Ω load, Fig. 6(c) and (g) show that currents are coupled to the radiator of PM 1 and flow to port 1. Moreover, in each of these cases, a certain amount of ground current also flows to the ground plane of the other PM via the short ground strip. The currents which come from the other PM result in high mutual coupling between the two ports.

With using the two ground stubs and port 1 excited, Fig. 6(b) shows that, at 4.5 GHz, significant amounts of current are coupled to the two stubs which serve as parasitic monopoles and give off radiation. As a result, the impedance bandwidth for S_{11} as shown in Fig. 5(a) is substantially extended towards the low frequency. The amounts of current coupled to the radiator of PM 2 and flowing to the ground plane of PM 2 via the short ground strip are less when compared with the case without the ground stubs in Fig. 6(a). These lead to low mutual coupling between the two ports. Similar phenomenon is observed at the frequency of 8.5 GHz as shown in Fig. 6(f), with the two ground stubs operating in the higher mode and generating the resonances at about 9 GHz for S_{11}, as shown in Fig. 5(a). The bandwidth is substantially extended towards the high frequency. The amounts of current coupled to the radiator of PM 2 and flowing on the ground plane of PM 2 are also less when compared with the case without the ground stubs in Fig. 6(e).

When port 2 is excited and at 4.5 GHz, Fig. 6(d) shows that significant amounts of currents are coupled to the two stubs which radiate the power. As a result, the lower cutoff frequency for S_{11} as shown in Fig. 5(b) is shifted down substantially. The currents coupled to the radiator of PM 2 and flowing to the ground plane of PM 2 via the short ground strip are less when compared with the case without the ground stubs in Figs. 6(c), resulting in low mutual coupling between the two ports. At the frequency of 8.5 GHz, the two ground stubs are operating in the higher mode as shown in Fig. 6(h). As shown in Fig. 5(b), the two stubs help generate the resonances at about 9 GHz and 10.25 GHz for S_{22}, shifting up the higher cutoff frequency substantially. The currents on the radiator and the ground plane of PM 1 are less when compared with the case without the ground stubs in Fig. 6(g). Thus, mutual coupling is significantly reduced. Note that Fig. 6 only shows the snap shots of the continuously changing current distributions.

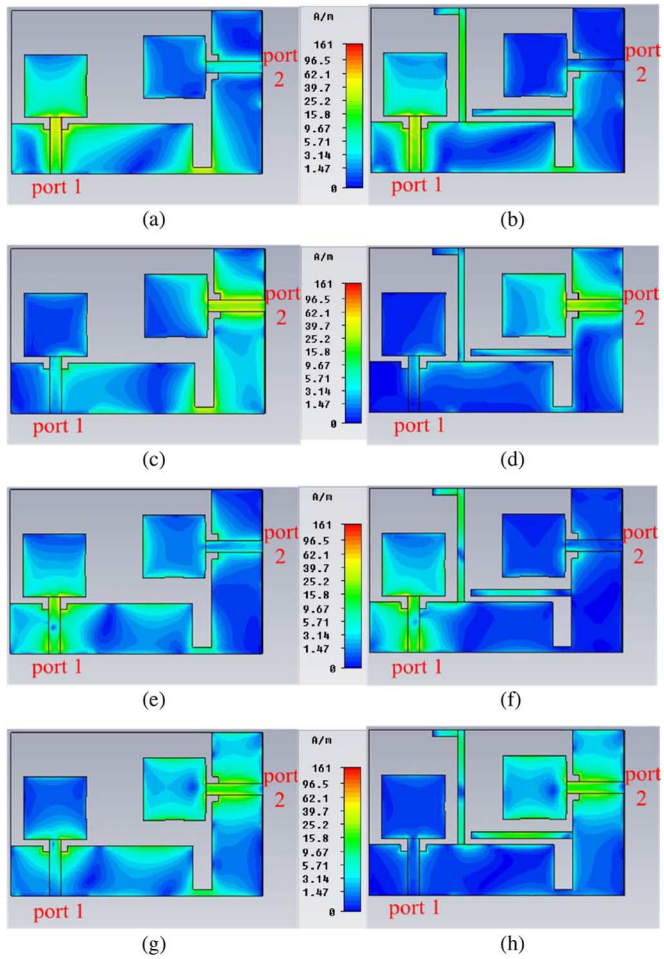

Fig. 6. Current distributions at 4.5 GHz: (a) Port 1 excited with no ground stub, (b) port 1 excited with ground stubs, (c) port 2 excited with no ground stubs, and (d) port 2 excited with ground stubs. Current distributions at 8.5 GHz: (e) Port 1 excited with no ground stub, (f) port 1 excited with ground stubs, (g) port 2 excited with no ground stubs, and (h) port 2 excited with ground stubs.

B. *Effects of Short Ground Strip*

In this study, the length L_{s3} of the short ground strip as shown in Fig. 1 is fixed at 3 mm, so that stubs 1 and 2 are not too close to each other, yet maintaining a small overall size for the MIMO antenna. With different values of W_{s3} and other dimensions having the values listed in Table 1, Fig. 7 shows the simulated S_{11}, S_{22} and S_{21}. It can be seen in Fig. 7(a) that W_{s3} does not have much effect on S_{11}. As W_{s3} decreases, Fig. 7(b) shows that the lower cutoff frequency for $S_{22} < -10$ dB reduces slightly. This is because the current flowing from PM 2 to PM 1 via the short ground strip is taking a longer route. Thus, using a narrower strip width W_{s3} can reduce the lower cutoff frequency slightly without increasing the radiator size. Fig. 7(c) shows that, with a decrease of W_{s3}, the resonances for S_{21} are shifted to the lower frequencies, with the lower resonance being farther away from the UWB. Since, within the UWB, the mutual coupling is lower with a smaller W_{s3}, in our design, W_{s3} is

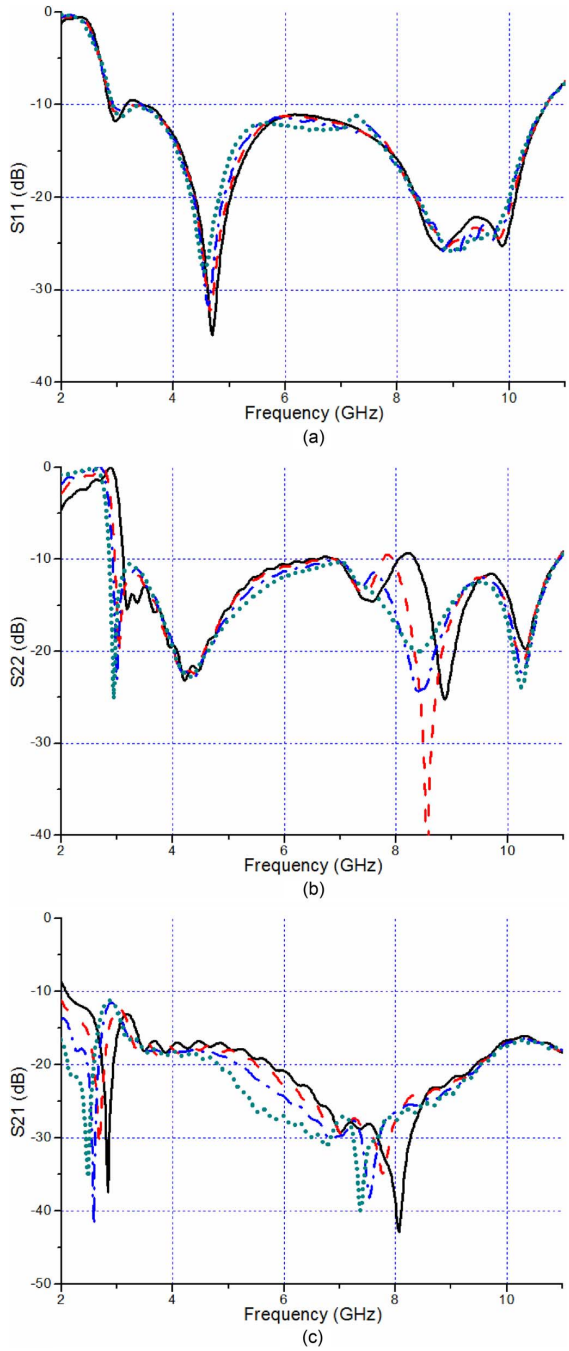

Fig. 7. Simulated (a) S_{11}, (b) S_{22}, and (c) S_{21} with different W_{s3}. ($\diamond\diamond\diamond\diamond\diamond$ $W_{s3} = 1$, — — — $W_{s3} = 3$, — — $W_{s3} = 5$, ——— $W_{s3} = 7$ mm).

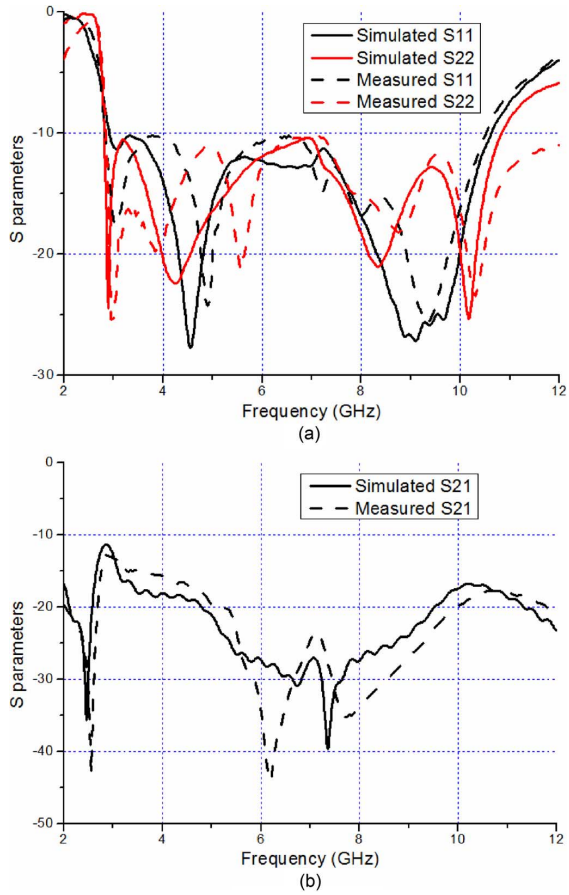

Fig. 8. Simulated and measured (a) S_{11} and S_{22}, and (b) S_{21}.

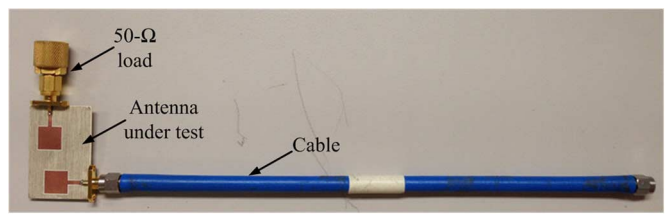

Fig. 9. Prototyped antenna with short feeding cable used in measurement.

set to a small value of 1 mm for achieving both wide bandwidth and low mutual coupling operations.

IV. Results and Discussions

A. S-Parameters

Computer simulation and measurement have been used to study the performance of the proposed MIMO antenna. The simulated and measured S_{11}, S_{22} and S_{21} of the final design are shown in Fig. 8, indicating good agreements between the simulated and measured results. The measured results in Fig. 8(a) show that port 1 has a bandwidth from 2.9 to 10.6 GHz for $S_{11} < -10$ dB, while port 2 has a bandwidth from 2.9 to more than 12 GHz for $S_{22} < -10$ dB. Thus, the antenna satisfies the impedance matching requirement for the entire UWB specified by the FCC. Mutual coupling of less than -15 dB is considered to be adequate for good performance [6], [10], [14], [15]. The simulated and measured S_{21} (mutual coupling) between the two input ports are shown in Fig. 8(b). The measured S_{21} is slightly worse than the simulated S_{21} at low frequencies from 3–5.5 GHz, mainly due to the effects of the connectors used in measurement. Fig. 8(b) shows that both the simulated and measured S_{21} are below -15 dB throughout the UWB, so the antenna is suitable for MIMO operation across the entire UWB band.

B. Radiation Patterns

The radiation pattern of the proposed MIMO antenna has been evaluated using computer simulation and measurement. In simulation, no feeding cable is needed to feed the signal to

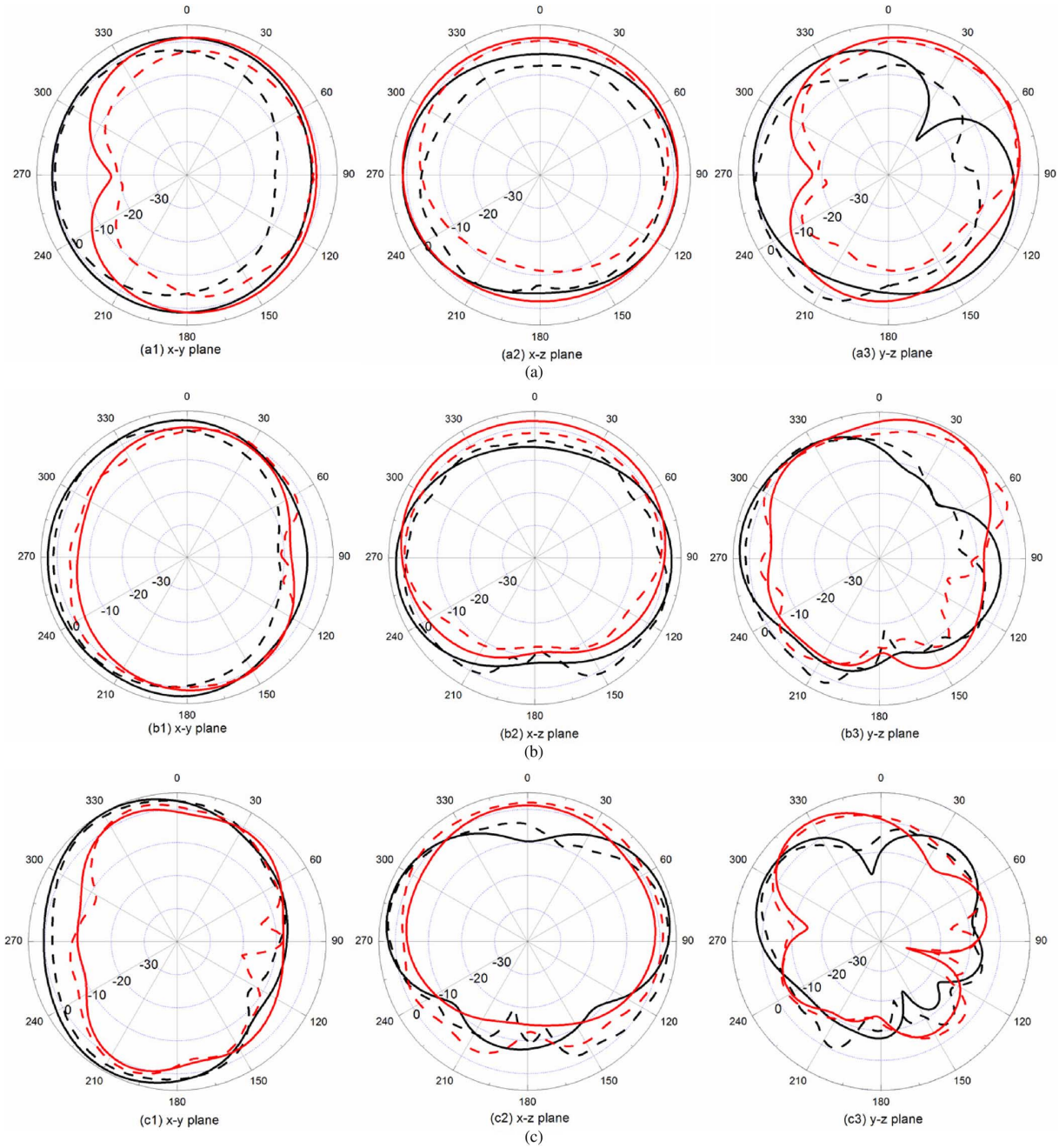

Fig. 10. Radiation patterns at (a) 3, (b) 7, and (c) 10 GHz (black: ——— simulated with port 1 excited; (black: - - - - - measured with port 1 excited; red: ——— simulated with port 2 excited; red: - - - - - measured with port 2 excited)

the antenna. However, in measurement, a short feeding cable as shown in Fig. 9 is needed to connect the antenna to the antenna measurement system, Satimo Starlab system. At low frequencies when the ground plane becomes electrically small, current will flow back from the antenna to the outer surface of the feeding cable, resulting in secondary radiation. The unwanted secondary radiation affects the measured radiation patterns and causes errors. Thus, to reduce the cable effects and produce more accurate results on radiation pattern measurement, the feeding cable provided by Satimo for use with the Starlab system is covered with EM suppressant tubing to absorb secondary radiation from the cable. However, with this approach, the measured gain of the antenna will be lower than the actual values, because some radiated power is absorbed by the EM suppressant tubing and does not get measured by the measurement system [17]. (It should be noted that in practice when the antenna is installed inside a wireless device, there will not be any cable effect because no cable is used.)

The simulated and measured realized gain radiation patterns of the antenna at the frequencies of 3, 7 and 10 GHz in the x-y, x-z and y-z planes are shown in Fig. 10(a), (b) and (c), respectively. Note that, in these figures, the x-y plane is the H-plane and E-plane for PM 1 and PM 2, respectively, while the x-z plane is the H-plane and E-plane of PM 2 and PM 1, respec-

tively. The radiation patterns in the y-z plane are used for discussion of pattern diversity later. In the study, when port 1 or 2 is excited, the other port is terminated with a 50-Ω load.

At the low frequency of 3 GHz when the ground plane becomes electrically smaller, Fig. 10(a1) and (a2) show that the measured radiation patterns are smaller than the simulated radiation patterns, which is caused by the feeding cable described previously. At this frequency, PM 1 and PM 2 have omnidirectional radiation patterns in the H-plane (i.e., in the x-y and the x-z planes, respectively), which is typical for monopole antennas. The radiation patterns in the E-plane are not dumb-bell shaped and do not have null, which are different from those of typical monopole antennas. This is because of the L-shaped common ground which makes the current distribution different from typical planar monopole. At the higher frequencies of 7 and 10 GHz when the cable effects are less, Fig. 10(b1), (b2), (c1) and (c2) show that the simulated and measured radiation patterns agree well. At 7 GHz, Fig. 10(b1) and (b2) show that PM 1 and PM 2 still have omnidirectional radiation patterns in the H-plane. However, at the higher frequency of 10 GHz, Fig. 10(c1) and (c2) shows that the radiation patterns in the H-plane are less omnidirectional because of higher-order resonant modes.

The realized peak gains of the antenna with ports 1 or 2 excited are shown in Fig. 11(a). It can be seen that the simulated and measured peak gains agree quite well. The measured gains range from 0.9 to 6.5 dBi across the frequency band from 2.9–10.6 GHz. The simulated and measured efficiencies of the antenna are shown in Fig. 11(b). It can be seen that the simulated efficiencies (without using the cable model described later) are above 80% across the UWB. The measured efficiencies are much less than the simulated efficiencies (without using the cable model), particularly at lower frequencies, which is due to effects of the feeding cable described earlier. To verify that the discrepancies are indeed caused by the effects of feeding cable, the simulation model for the feeding cable with EMI suppressant tubing developed in [17] is included in our simulation studies. The simulation results are shown in Fig. 11(b) for comparison. It can be seen that the measured and simulated efficiencies agree well, which verifies that the large discrepancies are caused by the feeding cable. (It should be noted that the feeding cable shown in Fig. 9 has also been used to measure the S parameters in all our studies. Since the simulated S parameters with and without using the cable model are similar in terms of bandwidths, for simplicity, only the simulated S parameters without using the cable are shown in this paper.)

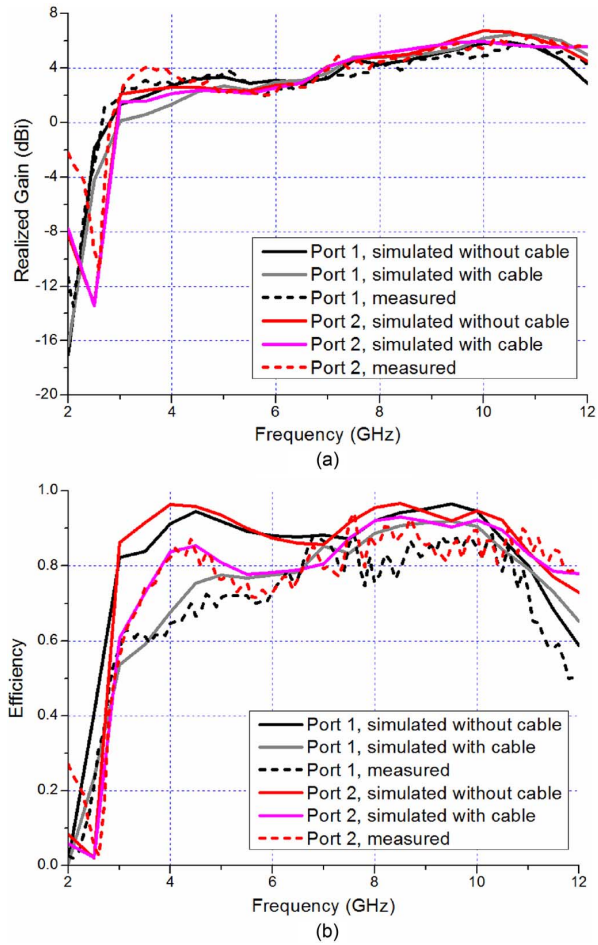

Fig. 11. (a) Realized gains and (b) efficiencies of MIMO antenna with port 1 or port 2 excited.

C. Diversity Performance

In pattern diversity, two or more different radiation patterns are employed to mitigate the effects of multipath and hence to reduce the probability of fading occurring simultaneously to all patterns at the same frequency. In our proposed MIMO antenna, the two PMs are placed perpendicularly to each other. This configuration results in two different radiation patterns as shown in Fig. 10 to receive signals from different directions, hence achieving pattern diversity. For example, the measured results in Fig. 10(a3) shows that, in the x-z plane, PM 1 has quite a small gain of -20 dB at the angle of 75°, but PM 2 has a gain of 0 dB at the same angle. At 270°, PM 2 has a null while PM 2 has a gain of 0 dB. This type of complementary patterns can also be observed in the y-z planes shown in Fig. 10(b3) and (c3), i.e., a null in the radiation pattern of one radiating element is always covered by the radiation pattern of the other radiating element. One of the basic requirements for antenna elements to be effectively used in pattern diversity is that their radiation patterns should be uncorrelated. The parameter used to assess the correlation between radiation patterns is the envelope correlation coefficient ρ_e, which can be calculated using the 3-D radiation patterns [18]. By assuming uniform 3-D angular power spectra, Eqn (7) in [18] is used to calculate the envelope correlation coefficient. With the uses of the measured and simulated radiation patterns of the proposed MIMO antenna, the calculated ρ_e are lower than 0.2 and 0.1, respectively, throughout the entire UWB. Usually when the two antenna elements have similar efficiencies, a good diversity performance can be achieved for $\rho_e < 0.7$ [12].

V. Conclusions

A MIMO antenna with a small size of 26×40 mm^2 for portable UWB applications has been proposed. The antenna consists of two PMs placed perpendicularly to each other to achieve good isolation between the input ports. Two long

ground stubs placed adjacent to the radiating elements and a short ground strip connecting the two ground planes together are employed to enhance the isolation. Simulated and measured results have shown that the antenna can operate in the entire UWB band from 3.1 to 10.6 GHz with mutual coupling of less than -15 dB between the two ports. The use of the antenna for pattern diversity has also been studied. Results have shown that the MIMO antenna can achieve an envelope correlation coefficient of less than 0.2 across the UWB. All results indicate that the MIMO antenna is a potential candidate for portable UWB applications.

REFERENCES

[1] Federal Communications Commission (FCC), Revision of Part 15 of the Commission's Rules Regarding Ultra-Wideband Transmission Systems First Rep. and Order, ET Docket 98-153, FCC 02-48, Adopted: Feb. 2002; Released, Apr. 2002.

[2] L. Zheng and C. Tse, "Diversity and multiplexing: A fundamental tradeoff in multiple-antenna channels," *IEEE Trans. Inf. Theory*, vol. 49, pp. 1073–1096, May 2003.

[3] K. L. Wong, S. W. Su, and Y. L. Kuo, "A printed Ultra-wideband diversity monopole antenna," *Microw. Opt. Technol. Lett.*, vol. 38, no. 4, pp. 257–259, 2003.

[4] L. Liu, H. Zhao, T. S. P. SEE, and Z. N. Chen, "A printed ultra-wideband diversity antenna," in *Proc. Int. Conf. on Ultrawideband (ICUWB'2006)*, Waltham, MA, USA, Sep. 2006, pp. 351–356.

[5] S. Hong, K. Chung, J. Lee, S. Jung, S. S. Lee, and J. Choi, "Design of a diversity antenna with stubs for UWB applications," *Microw. Opt. Technol. Lett.*, vol. 50, no. 5, pp. 1352–1356, 2008.

[6] S. Zhang, Z. Ying, J. Xiong, and S. He, "Ultrawideband MIMO/diversity antennas with a tree-like structure to enhance wideband isolation," *IEEE Antennas Wireless Propag. Lett.*, vol. 8, pp. 1279–1282, 2009.

[7] T. S. P. See and Z. N. Chen, "An ultrawideband diversity antenna," *IEEE Trans. Antennas Propag.*, vol. 57, no. 6, pp. 1597–1605, 2009.

[8] Y. Cheng, W. J. Lu, and C. H. Cheng, "Printed diversity antenna for ultra-wideband applications," in *Proc. Int. Conf. Ultrawideband (ICUWB'2010)*, Nanjing, China, Sep. 2010, pp. 1–4.

[9] H. K. Yoon, Y. J. Yoon, H. Kim, and C. H. Lee, "Flexible ultra-wideband polarisation diversity antenna with band-notch function," *IET Microw. Antennas. Propag.*, vol. 5, no. 12, pp. 1463–1470, 2011.

[10] J. M. Lee, K. B. Kim, H. K. Ryu, and J. M. Woo, "A compact ultrawideband MIMO antenna with WLAN band-rejected operation for mobile devices," *IEEE Antennas Wireless Propag. Lett.*, vol. 11, pp. 990–993, 2012.

[11] A. Rajagopalan, G. Gupta, A. S. Konanur, B. Hughes, and G. Lazzi, "Increasing channel capacity of an ultrawideband MIMO system using vector antennas," *IEEE Trans. Antennas Propag.*, vol. 55, no. 10, pp. 2880–2887, 2007.

[12] S. Zhang, B. K. Lau, A. Sunesson, and S. He, "Closely-packed UWB MIMO/diversity antenna with different patterns and polarizations for USB dongle applications," *IEEE Trans. Antennas Propag.*, vol. 60, no. 9, pp. 4372–4380, 2012.

[13] G. Adamiuk, S. Beer, W. Wiesbeck, and T. Zwick, "Dual-orthogonal polarized antenna for UWB-IR technology," *IEEE Antennas Wireless Propag. Lett.*, vol. 8, pp. 981–984, 2009.

[14] E. A. Daviu, M. Gallo, B. B. Clemente, and M. F. Bataller, "Ultra-wideband slot ring antenna for diversity applications," *Electron. Lett.*, vol. 46, no. 7, pp. 478–480, 2010.

[15] M. Gallo, E. A. Daviu, M. F. Bataller, M. Bozzetti, J. M. Pardo, and L. J. Llacer, "A broadband pattern diversity annular slot antenna," *IEEE Trans. Antennas Propag.*, vol. 60, no. 3, pp. 1596–1600, 2012.

[16] Y. C. Lu and Y. C. Lin, "A compact dual-polarized UWB antenna with high port isolation," in *Proc. IEEE Antennas Propag. Society Int. Symp. (APSURSI'2010)*, Toronto, ON, Canada, Jul. 2010.

[17] L. Liu, S. W. Cheung, Y. F. Weng, and T. I. Yuk, M. A. Matin, Ed., "Cable effects on measuring small planar UWB monopole antennas," *Ultra Wideband—Current Status and Future Trends*, Oct. 2012.

[18] M. B. Knudsen and G. F. Pedersen, "Spherical outdoor to indoor power spectrum model at the mobile terminal," *IEEE J. Sel. Areas Commun.*, vol. 20, no. 6, pp. 1156–1168, Aug. 2002.

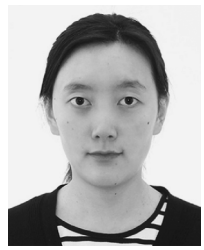

Li Liu received the B.Sc. degree in electronic information science and technology from the University of Electronic Science and Technology of China, Chengdu, China, in 2009.

From 2009 to 2010, she pursued graduate study in electromagnetic field and microwave at Southeast University, Nanjing, China. She is currently working toward the Ph.D. degree in electrical and electronic engineering at the University of Hong Kong, Hong Kong, China. Her research interests include RF and microwave circuits, small antennas, and MIMO systems.

S. W. Cheung (SM'96) received the B.Sc. degree (first class hons) in electrical and electronic engineering from Middlesex University, U.K., in 1982 and the Ph.D. degree from Loughborough University of Technology, U.K., in 1986.

From 1982 to 1986, he was a research assistant in the Department of Electronic and Electrical Engineering at Loughborough University of Technology, where he collaborated with Rutherford Appleton Laboratory and many U.K. universities to work a project for new generations of satellite systems. He is an Associate Professor at the University of Hong Kong and in charge of the Microwave, RF Frequency and Telecom Laboratories. His current research interests include antenna designs, 2G, 3G, and 4G mobile communications systems, MIMO systems and satellite communications systems.

Prof. Cheung has been serving the IEEE in Hong Kong for the past 20 years. In 2009 and 2010, he was the Chairman of the IEEE Hong Kong Joint Chapter on Circuits and Systems and Communications. He was the Honorary Treasurer and currently the Chair-Elect of the IEEE Hong Kong.

T. I. Yuk received the B.S. degree from Iowa State University, Ames, IA, USA, in 1978 and the M.S. and Ph.D. degrees from Arizona State University, Tempe, AZ, USA, in 1980 and 1986, respectively.

Since 1986, he has been teaching at the University of Hong Kong. His current research interests include: wireless communications and antenna designs.